Wavelength bistability based on optical injection in a novel tunable dual mode laser

Hang Zhao,[1] Yao Zhu,[1] Feng Li,[2] and Yonglin Yu[1*]

[1]*Wuhan National Laboratory for Optoelectronics, Huazhong University of Science and Technology, Wuhan 430074, China*

[2]*Photonics Research Centre, Department of Electronic and Information Engineering, The Hong Kong Polytechnic University, Hong Kong, China*

[*]*yonglinyu@mail.hust.edu.cn*

Abstract: A novel tunable dual mode laser is proposed based on a double-layer Bragg grating structure, named double-layer grating distributed Bragg reflector (DLG-DBR) laser. With controlling the gain saturation condition, different oscillating states can be observed. The nonlinear dynamics characteristics including bifurcation of the laser under optical injection with two different start-up sequences are analyzed with numerical simulations. Furthermore, we investigate the lasing wavelength bistability of the laser combined with its tuning characteristics theoretically. Optical memory operation based on the external optical injection locking bistability of the dual mode device is proposed. The memory operation can be achieved in the whole wavelength window with a 10 nm tuning range. A mode suppression ratio (MSR) of more than 45 dB is achieved between the two bistable states.

OCIS codes: (140.3600) Lasers, tunable; (140.3520) Lasers, injection-locked; (190.1450) Bistability; (230.1150) All-optical devices.

References and links

1. S. Osborne, K. Buckley, A. Amann, and S. O'Brien, "All-optical memory based on the injection locking bistability of a two-color laser diode," Opt. Express **17**(8), 6293–6300 (2009).
2. C. Laperle, M. Svilans, M. Poirier, and M. Tetu, "Frequency multiplication of microwave signals by sideband optical injection locking using a monolithic dual-wavelength DFB laser device," IEEE Trans. Microw. Theory Tech. **47**(7), 1219–1224 (1999).
3. P. Heinricht, N. Brandonisio, S. O'Brien, and S. Osborne, "Fast Wavelength Switching of a Dual-Contact Two-Color Semiconductor Laser With Current Modulation," IEEE Photonics Technol. Lett. **23**(8), 513–515 (2011).
4. F. Pozzi, R. M. De La Rue, and M. Sorel, "Dual-Wavelength InAlGaAs–InP Laterally Coupled Distributed Feedback Laser," IEEE Photonics Technol. Lett. **18**(24), 2563–2565 (2006).
5. S. D. Roh, T. S. Yeoh, R. B. Swint, A. E. Huber, C. Y. Woo, J. S. Hughes, and J. J. Coleman, "Dual-Wavelength InGaAs–GaAs Ridge Waveguide Distributed Bragg Reflector Lasers with Tunable Mode Separation," IEEE Photonics Technol. Lett. **12**(10), 1307–1309 (2000).
6. S. Shutts, P. M. Smowton, and A. B. Krysa, "Dual-wavelength InP quantum dot lasers," Appl. Phys. Lett. **104**(24), 241106 (2014).
7. R. K. Price, V. B. Verma, K. E. Tobin, V. C. Elarde, and J. J. Coleman, "Y-Branch Surface-Etched Distributed Bragg Reflector Lasers at 850 nm for Optical Heterodyning," IEEE Photonics Technol. Lett. **19**(20), 1610–1612 (2007).
8. P. K. A. Wai, L. Xu, L. F. K. Lui, L. Y. Chan, C. C. Lee, H. Y. Tam, and M. S. Demokan, "All-optical add-drop node for optical packet-switched networks," Opt. Lett. **30**(12), 1515–1517 (2005).
9. Y. Luo, F. Li, J. Liu, L. Gan, C. Lu, and K. A. W. Ping, "10-Gb/s All-Optical VPN in WDM-PON Using Injection-Locked Fabry–Pérot Laser Diodes," IEEE Photonics Technol. Lett. **26**(22), 2299–2302 (2014).
10. L. Gan, J. Liu, F. Li, and P. K. A. Wai, "An Optical Millimeter-wave Generator Using Optical Higher-order Sideband Injection Locking in a Fabry-Pérot Laser Diode," J. Lightwave Technol. **33**(23), 4985–4996 (2015).
11. A. Hurtado, M. Nami, I. D. Henning, M. J. Adams, and L. F. Lester, "Two-Wavelength Switching With a 1310-nm Quantum Dot Distributed Feedback Laser," IEEE J. Sel. Top. Quantum Electron. **19**(4), 1900708 (2013).
12. K. Huybrechts, G. Morthier, and R. Baets, "Fast all-optical flip-flop based on a single distributed feedback laser diode," Opt. Express **16**(15), 11405–11410 (2008).

#256191 Received 21 Dec 2015; revised 2 Feb 2016; accepted 5 Feb 2016; published 16 Feb 2016

13. K. Inoue and M. Yoshino, "Bistability and wave-form reshaping in a DFB-LD with side-mode light injection," IEEE Photonics Technol. Lett. **7**(2), 164–166 (1995).
14. I. Gatare, M. Sciamanna, J. Buesa, H. Thienpont, and K. Panajotov, "Nonlinear dynamics accompanying polarization switching in vertical-cavity surface-emitting lasers with orthogonal optical injection," Appl. Phys. Lett. **88**(10), 101106 (2006).
15. A. Hurtado, A. Quirce, A. Valle, L. Pesquera, and M. J. Adams, "Nonlinear dynamics induced by parallel and orthogonal optical injection in 1550 nm Vertical-Cavity Surface-Emitting Lasers (VCSELs)," Opt. Express **18**(9), 9423–9428 (2010).
16. R. Al-Seyab, K. Schires, N. A. Khan, A. Hurtado, I. D. Henning, and M. J. Adams, "Dynamics of Polarized Optical Injection in 1550-nm VCSELs: Theory and Experiments," IEEE J. Sel. Top. Quantum Electron. **17**(5), 1242–1249 (2011).
17. K. Huybrechts, R. Baets, and G. Morthier, "All-Optical Flip-Flop Operation in a Standard Tunable DBR Laser Diode," IEEE Photonics Technol. Lett. **21**(24), 1873–1875 (2009).
18. T. Kakitsuka, S. Matsuo, K. Hamamoto, T. Segawa, H. Suzuki, and R. Takahashi, "Injection-Locked Flip-Flop Operation of a DBR Laser," IEEE Photonics Technol. Lett. **23**(17), 1261–1263 (2011).
19. H. Kawaguchi, "Bistable Laser Diodes and Their Applications: State of the Art," IEEE J. Sel. Top. Quantum Electron. **3**(5), 1254–1270 (1997).
20. A. Murakami, "Phase Locking and Chaos Synchronization in Injection-Locked Semiconductor Lasers," IEEE J. Quantum Electron. **39**(3), 438–447 (2003).
21. E. K. Lau, H.-K. Sung, and M. C. Wu, "Frequency Response Enhancement of Optical Injection-Locked Lasers," IEEE J. Quantum Electron. **44**(1), 90–99 (2008).
22. L. Zhang and J. C. Cartledge, "Fast Wavelength Switching of Three-Section DBR Lasers," IEEE J. Quantum Electron. **31**(1), 75–81 (1995).
23. H. Zhao, S. Hu, J. Zhao, Y. Zhu, Y. Yu, and L. P. Barry, "Chirp-Compensated DBR Lasers for TWDM-PON Applications," IEEE Photonics J. **7**(1), 7900809 (2015).
24. J. Zhao, S. Hu, Y. Tang, H. Zhao, and Y. Yu, "Widely Tunable Semiconductor Laser Based on Digital Concatenated Grating With Multiple Phase Shifts," IEEE Photonics J. **5**(5), 1502008 (2013).
25. M. M. Krstić, J. V. Crnjanski, and D. M. Gvozdic, "Injection Power and Detuning-Dependent Bistability in Fabry-Perot Laser Diodes," IEEE J. Sel. Top. Quantum Electron. **18**(2), 826–833 (2012).
26. A. Murakami, "Synchronization of chaos due to linear response in optically driven semiconductor lasers," Phys. Rev. E Stat. Nonlin. Soft Matter Phys. **65**(5), 056617 (2002).
27. T. Erneux, V. Kovanis, A. Gavrielides, and P. M. Alsing, "Mechanism for period-doubling bifurcation in a semiconductor laser subject to optical injection," Phys. Rev. A **53**(6), 4372–4380 (1996).
28. S. Wieczorek, B. Krauskopf, T. B. Simpson, and D. Lenstra, "The dynamical complexity of optically injected semiconductor lasers," Phys. Rep. **416**(1-2), 1–128 (2005).
29. E. K. Lau, L. J. Wong, and M. C. Wu, "Enhanced Modulation Characteristics of Optical Injection-Locked Lasers: A Tutorial," IEEE J. Sel. Top. Quantum Electron. **15**(3), 618–633 (2009).
30. Y. An, A. L. Riesgo, C. Peucheret, and G. Morthier, "Wavelength Tunable Flip-Flop Operation of a Modulated Grating Y-branch Laser," Proceedings of International Conference on Photonics in Switching, (Ajaccio, 2012), pp. 1–4.

1. Introduction

Dual mode or wavelength lasers have attracted intense research interest due to their potential applications in all-optical signal processing, photonic generation of microwave, terahertz (THz) imaging and optical remote sensing [1, 2]. A variety of effective methods have been developed to realize such devices. A slotted Fabry–Pérot diode laser is designed by introducing a small number of localized refractive index perturbations along cavity to support only two primary modes [3]. An additional index step features in this device is needed and must be precisely designed. Laterally coupled distributed feedback (DFB) laser with dual-wavelength emitting which has two different grating periods, one on each sidewall has been reported in [4]. In order to overcome limitations of wavelength tuning of these lasers, the distributed Bragg reflectors (DBRs) are cascaded to realize dual-wavelength emitting [5, 6]. Although these devices are wavelength tunable, two set of cavity modes with different channel spacing can exist in the cavity which make them difficult to meet ITU recommendation. An effort to combine the two wavelengths into a single emitting arm has been achieved using Y-branch lasers [7]. The challenge of these devices is that they have a larger footprint than normal laser diodes and require careful design of the out-coupler to prevent back-reflections into opposing arms of the Y-branch, which otherwise creates instability in the output.

#256191 Received 21 Dec 2015; revised 2 Feb 2016; accepted 5 Feb 2016; published 16 Feb 2016

Semiconductor lasers exhibiting wavelength bistability are attractive candidates as optical bistability components in the next generation optical networks [8–10]. Various types of bistable semiconductor lasers have been demonstrated in previous studies. Wavelength bistability in DFB lasers have recently become a focus of extensive research because of its wide potential applications, including all-optical logic gates, wavelength switching [11], all-optical flip-flop operation [12] and optical signal regeneration [13]. Different phenomena in optical injected vertical cavity surface emitting lasers (VCSELs), such as polarization bistability and switching [14], nonlinear dynamics [15], and the stability with polarized injection [16] have also been studied. Recently, all-optical flip-flop operations in DBR lasers were experimentally demonstrated by using the bistability of injection locking when pulses with either different durations and amplitudes [17] or different wavelengths [18] are injected. However, the wavelength bistability of such DBR lasers and the tuning characteristics have not been well studied.

In this paper, a novel tunable dual mode laser is proposed based on a double-layer Bragg grating (DLG) structure, named DLG-DBR laser. The spacing of the two lasing modes can be engineered with the double grating periods and wavelength tunability can be achieved by tuning the drive current. With different gain saturation conditions, the laser can operate at different oscillating states with dual modes or single mode. In the case of moderate coupling (cross-saturation coefficient equal self-saturation coefficient), the two modes can lase in turns with changing of the tuning currents. Bifurcation characteristics of the laser output are then analyzed by numerical simulations with different start-up sequences and different gain saturation conditions. Wavelength bistability of the laser combined with its tuning characteristics are then investigated. Finally, with external optical injection locking, optical memory operations based on the proposed dual mode device are demonstrated.

2. Structure design and characteristics of DLG-DBR laser

The schematic of the proposed laser is shown in Fig. 1(a). As compared with typical three section DBR lasers, the most significant difference in the proposed laser is that two sections of Bragg gratings with different periods (Λ_1 and Λ_2) are etched on the upper and lower surfaces of the waveguide, respectively. Thus two peaks are achieved on the reflectivity spectrum, as shown in Fig. 1(b). The spacing of the two reflection peaks $\Delta\lambda_B$ is governed by $2n_{eff}(\Lambda_1\text{-}\Lambda_2)$, where n_{eff} is the effective refractive index of the double layer Bragg grating. The designed grating can be characterized in COMSOL to optimize the parameters such as periods, depth and total length. For example, we design a laser whose active, phase and grating sections have lengths 250 μm, 100 μm and 400 μm, respectively, and with double grating periods Λ_1 = 228 nm and Λ_2 = 229 nm. As a result, the spacing of the two lasing modes is 7.2 nm which is 9 times of the longitudinal mode spacing 0.8 nm of the laser cavity. The DLG is used here as a mirror, so the laser cavity is defined by the facet in the left side of the active section and the DLG.

#256191 Received 21 Dec 2015; revised 2 Feb 2016; accepted 5 Feb 2016; published 16 Feb 2016

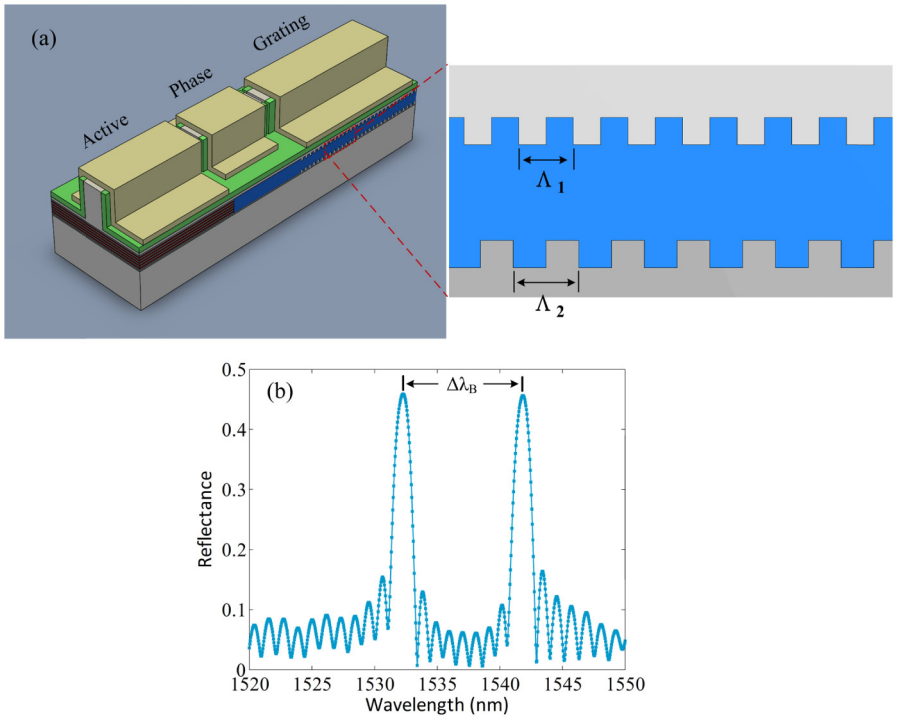

Fig. 1. (a) Schematic of the DLG-DBR laser. (b) The reflectivity spectrum of the double-layer Bragg grating with double grating periods Λ_1 = 228 nm and Λ_2 = 229 nm.

In a dual mode semiconductor laser, the primary parameter that determines the nature of mode competition dynamics is the mode coupling constant, which is defined as the ratio of cross- and self-saturation coefficients (ε_{self} *and* ε_{cross}) [19]. We have developed a simulation model (with MATLAB) to describe characteristics of the proposed dual mode laser. The details of the model will be presented in Section 3.1, including the case of optical injection. Here, some numerical simulations without optical injection, are presented to describe wavelength tuning characteristics and mode competition dynamics of the DLG-DBR laser. In our numerical investigations, 16 longitudinal modes are considered with a flat gain profile. Hence the lasing modes are determined by only the double-layer grating. Figure 2 presents the flow diagrams of mode-1 and mode-2 in two possible characteristic situations, strong and weak coupling, at different phase currents I_p. For strong mode coupling ($\varepsilon_{self} < \varepsilon_{cross}$), only one mode can oscillate, the other will be suppressed as shown in Fig. 2(a). In this case, the current applied on the phase section determines the choice from the bistable states A and B, that the laser will finally reach. However, if the mode coupling is weak ($\varepsilon_{self} > \varepsilon_{cross}$), the two longitudinal modes of the laser will survive simultaneously in the cavity, and the intensity ratio of the two modes will change along the variation of the phase current as shown in Fig. 2(b). We can observe that the laser oscillates and converges to state B′ for both I_p = 4.1 mA and I_p = 4.2 mA because of the almost equal threshold gains for mode-1 and mode-2. In contrary, such slight difference between the threshold gains of mode-1 and mode-2 for I_p = 4.1 mA and I_p = 4.2 mA has leaded the laser to significantly different lasing states in strong coupling case as shown in Fig. 2(a).

#256191 Received 21 Dec 2015; revised 2 Feb 2016; accepted 5 Feb 2016; published 16 Feb 2016

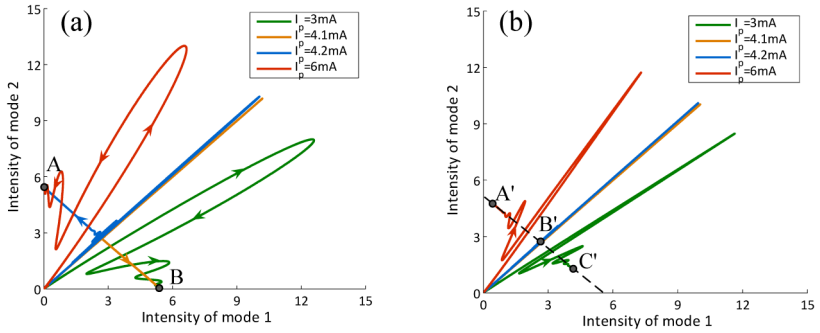

Fig. 2. Flow diagrams of two-mode competition for (a) strong coupling ($\varepsilon_{self} = 0.7 \times 10^{-23}$ m^3, $\varepsilon_{cross} = 1 \times 10^{-23}$ m^3) and (b) weak coupling ($\varepsilon_{self} = 1 \times 10^{-23}$ m^3, $\varepsilon_{cross} = 0.7 \times 10^{-23}$ m^3) at four different phase currents I_p.

From Fig. 2, it has been shown that the final state of the dual mode semiconductor laser is sensitive to the drive current of the phase section. Besides the phase current, other parameters such as the drive current of the grating section are also important to determine the final state. To investigate how such parameters determine the laser state, we choose a particular case with moderate coupling, where $\varepsilon_{self} = \varepsilon_{cross} = 1 \times 10^{-23}$ m^3. Such moderate coupling case is representative since the dynamics in either strong coupling or weak coupling cases can both be observed in this case.

The wavelength tuning and power variations of the two lasing modes along the increases of phase current and grating current are shown in Fig. 3. The results with different drive currents are obtained independently in simulations so the memory effect in bistable system is not included. Figure 3(a) and 3(b) show the tuning of peak positions of the lasing modes in the cavity with increases of phase current and grating current respectively. The grating current is fixed to 10 mA in Fig. 3(a) and the phase current is fixed to 6 mA in Fig. 3(b). The red circle marks indicate the higher power one among the two lasing modes and the blue circle marks represent the lower power mode. In Fig. 3(a), the longitudinal modes shift to blue side with the increasing of phase current, within one longitudinal mode spacing. Multiple mode hoppings can be observed in the whole tuning process. From Fig. 1(b), we know that the 3dB bandwidth of the two DLG reflection peaks is comparable to the longitudinal mode spacing and more than one longitudinal modes are covered by each DLG reflection profile. Along the phase current tuning, the longitudinal mode which is originally the dominant mode under a DLG reflection profile will be tuned away from the peak of the DLG reflection profile. At the same time, the next longitudinal mode will be tuned into the DLG reflection profile and replace the original dominant mode. In the mode tuning process, the peak position of the new dominant longitudinal mode will sweep from the red side to the blue side of the DLG reflection profile. When the peaks of the dominant longitudinal mode and the DLG reflection profile overlap in the tuning process, this longitudinal mode will see the maximal net gain in the cavity and suppress all other longitudinal modes. In Fig. 3(a), after each mode hopping point, that DLG new emerged mode will become the higher power mode when the phase current is further increased. Figure 3(c) demonstrates the power variations of the two lasing modes along the increasing of phase current. The powers of the two lasing modes are plotted in blue and orange solid curves and the cross points of them are accordant to the mode switching points shown in Fig. 3(a). It should be noted that the mode switching regions indicated by the rising and falling parts of the curves in Fig. 3(c) will be narrowed in the strong coupling case and broaden in the weak coupling case. In the strong coupling case, the flat top parts of the power curves shown in Fig. 3(c) will be dominant so the working points of the laser will be close to either the abscissa or the ordinate of the flow diagram as shown in Fig. 2(a). In contrary, the flat top parts of the power curves will be narrowed in the weak

#256191 Received 21 Dec 2015; revised 2 Feb 2016; accepted 5 Feb 2016; published 16 Feb 2016

coupling case and the working points will locate far from the axes in most time as shown in Fig. 2(b).

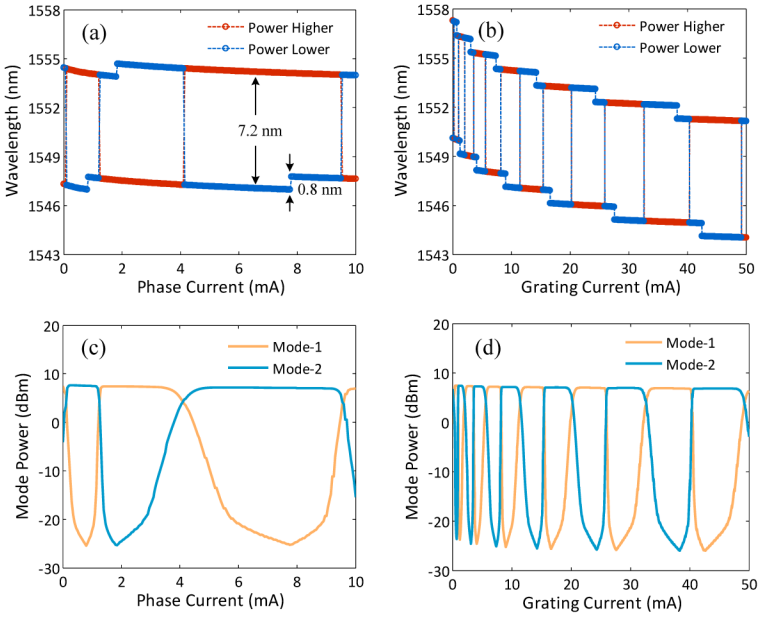

Fig. 3. The wavelength tuning characteristics of the laser in the moderate coupling case ($\varepsilon_{self} = \varepsilon_{cross} = 1 \times 10^{-23}$ m^3). (a) and (b) show variations of the peak positions of the two lasing modes with the increasing of phase current and grating current, respectively. The higher and lower power modes are indicated by red and blue circle marks. (c) and (d) show the power variations of the two lasing modes versus phase current and grating current respectively. The grating current is fixed to 10 mA in (a) and (c) and the phase current is fixed to 6 mA in (b) and (d).

In Fig. 3(a), the grating current is fixed so the positions of the two DLG reflection peaks strongly confine the wavelengths of the lasing modes. When the grating current is tuned, as shown in Fig. 3(b), the wavelengths of the two lasing modes are significantly shifted. The mode hopping in Fig. 3(b) is similar to that in Fig. 3(a) but this time the lasing modes hop from long wavelength to short wavelength. With the increasing of grating current, the positions of the cavity longitudinal modes are also slightly shifted but the mode hopping is still the dominant way of wavelength tuning. Comparing with the less than 1 nm wavelength tuning in Fig. 3(a), the wavelength shift induced by grating current tuning is larger than 6 nm. It is possible to achieve 10 nm tuning rang by increasing the grating section current.

3. Injection locking of DLG-DBR laser

Optical injection-locking (OIL) is an efficient method to achieve wavelength bistability in laser diodes (LDs). A typical schematic for injection locking of the DLG-DBR laser is shown in Fig. 4. The continuous wave (CW) output of a tunable single frequency laser, which is the master laser (ML), is injected into the DLG-DBR laser, which is the slave laser (SL), via a circulator. The amplitude of the CW signal is adjusted by a variable optical attenuator (VOA). The polarization state of the CW signal is aligned to the output of DLG-DBR by the polarization controller (PC) before the circulator. The output of the DLG-DBR laser is detected by an optical spectrum analyzer (OSA). To investigate the responses of the DLG-DBR laser to different optical injections, a numerical model based on coupled differential equations is used to describe the dynamics of the laser cavity modes. Then the stable injection locking, bistability, self-pulsing and related bifurcations are investigated and discussed.

#256191 Received 21 Dec 2015; revised 2 Feb 2016; accepted 5 Feb 2016; published 16 Feb 2016

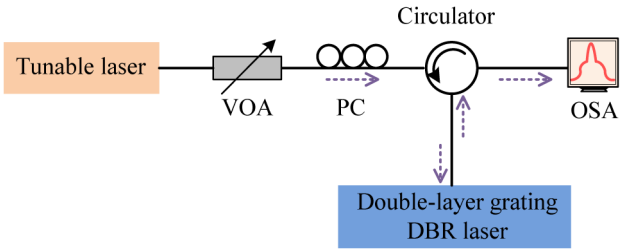

Fig. 4. A representative configuration of an optical injected double-layer grating DBR laser.

3.1 Theoretical model

The differential equations governing the dynamics of the complex electrical fields of the laser modes in a laser with optical injections are similar to those of a free-running laser, with additional injection terms [20, 21]. We partially modify it by introducing terms of spontaneous emission and gain saturation as

$$\frac{dE_m}{dt}=\frac{1}{2}(1+i\alpha)\left[\frac{G_n(N-N_0)}{1+\sum_j \varepsilon_{m,j}S_j}-\frac{1}{\tau_m}+\frac{\beta_{sp}R_{sp}}{S_m}\right]E_m+\kappa A_{inj}\exp(i\Delta\omega_m t), \qquad (1)$$

where E_m is the complex amplitude of the m-th cavity mode of the slave laser. The linewidth enhancement factor α is fixed to a typical value 3 in simulations. G_n is the differential gain coefficient with fixed value 1×10^{-12} m^3/s and the transparent carrier density N_0 is 1.3722×10^{24} m^{-3} in simulations. The gain saturation is determined by the summation of the weighted photon densities $\varepsilon_{m,j}S_j$, where $\varepsilon_{m,j}$'s are the gain saturation factors and S_j is the photon density of j-th cavity mode. Specifically, the gain saturation factor $\varepsilon_{m,j} = \varepsilon_{self}$ when $m = j$ and $\varepsilon_{m,j} = \varepsilon_{cross}$ when $m \neq j$, where ε_{self} and ε_{cross} stand for the strengths of self- and cross-saturation, respectively. τ_m is the photon lifetime of the m-th cavity mode which has included the additional loss in the filtering of the DLG. The longitudinal or cavity modes have different photon lifetimes in the cavity because of the different reflectivity they got from the DLG reflection profile. When different phase current I_p and grating current I_g are injected to the laser, all cavity modes and the DLG reflection profile will be shifted due to carrier-induced index change in phase and grating section [22]. Therefore, photon lifetime τ_m for m-th longitudinal mode can vary significantly with the tuning of phase and grating currents. R_{sp} is the total spontaneous emission rate and β_{sp} defines the proportion of that falls into an individual cavity mode. The injection signal is described as $A_{inj}\exp(i\Delta\omega_m t)$ where $\Delta\omega$ is the angular frequency detuning of the injection light from the target mode of the free running slave laser. κ denotes the coupling rate expressed in the form of $(1-r_0^2)(r_0T)^{-1}$, where T is the cavity round-trip time, r_0 represents the amplitude reflectivity of the laser output facet. The dynamics of the carrier density can be modeled by the following equation with coupling to the photon densities of all cavity modes:

$$\frac{dN}{dt}=\frac{I_a}{qV}-\left(AN+BN^2+CN^3\right)-\sum_n \frac{G_n(N-N_0)S_n}{1+\sum_k \varepsilon_{n,k}S_k}, \qquad (2)$$

where I_a is the drive current to the active section of the DLG-DBR laser, q is the electron charge and V is the volume of active section. The second term in the bracket includes the recombination losses of carrier. The last term is the total carrier depletion of the stimulated emission in optical amplification of all cavity modes. The coupled Eqs. (1) and (2) can describe all of the dynamics of the cavity modes and carrier density in time domain.

Besides the numerical simulations of the dynamics based on (1) and (2), the system can also be characterized by the steady state solutions which can be found if the amplitude Eq. (1)

#256191 Received 21 Dec 2015; revised 2 Feb 2016; accepted 5 Feb 2016; published 16 Feb 2016

for $E_m = S_m^{1/2}\exp(i\varphi_m)$ is split into coupled equations to describe the photon density and the phase separately as

$$\frac{dS_m}{dt} = \left[\frac{G_n(N-N_0)}{1+\sum_j \varepsilon_{m,j}S_j} - \frac{1}{\tau_m}\right]S_m + 2\kappa\sqrt{S_{inj}S_m}\cos\phi_m + \beta_{sp}R_{sp}, \tag{3}$$

$$\frac{dS_k}{dt} = \left[\frac{G_n(N-N_0)}{1+\sum_j \varepsilon_{k,j}S_j} - \frac{1}{\tau_k}\right]S_k + \beta_{sp}R_{sp}, \tag{4}$$

$$\frac{d\phi_m}{dt} = \frac{\alpha}{2}\left[\frac{G_n(N-N_0)}{1+\sum_j \varepsilon_{m,j}S_j} - \frac{1}{\tau_m}\right] - \kappa\sqrt{\frac{S_{inj}}{S_m}}\sin\phi_m - \Delta\omega \tag{5}$$

where $\phi_m = \varphi_m - \omega t$ is the phase difference between the internal and injected fields. The values of parameters used in the coupled equations are listed in Table 1 [23, 24]. The cavity modes without injection are calculated only by the photon density equations since the phases of them coupled to the system can be neglected. The carrier density will still be governed by Eq. (2). When the slave laser is injection locked to the injection light, the steady-state solutions for the variables can be solved by setting the left-hand side terms of Eqs. (2)-(5) to zero [20, 21, 25]. Linear stability analysis will be further applied to the steady-state solutions to determine the stable locking regions of the system [26].

Table 1. The values of parameters used in the model

Active section length, l_a	250 μm
Active section width, w_a	1.2 μm
Active Section thickness, d_a	0.18 μm
Effective refractive index, n_{eff}	3.4
Group refractive index, n_g	3.56
Nonradiative recombination coefficient, A	1×10^8/s
Radiative recombination coefficient, B	8×10^{-17}m^3/s
Auger recombination coefficient in active section, C_a	7.5×10^{-41}m^6/s
Differential gain coefficient, G_n	1×10^{-12}m^3/s
Transparent carrier density, N_0	1.3722×10^{24}/m^3
Linewidth enhancement factor, α	3
Facet reflectivity, r_0^2	0.32
Spontaneous emission factor, β_{sp}	1×10^{-4}
Phase section length, l_p	120 μm
Grating section length, l_g	400 μm
Passive section thickness, d_p	0.3 μm
Auger recombination coefficient in passive sections, C_p	4×10^{-41}m^6/s
Normalized coupling coefficient, ζl_g	2
Grating period, Λ_1	228 nm
Grating period, Λ_2	229 nm

3.2 Characterization of injection locking in DLG-DBR laser

The OIL system has two primary parameters: one is the strength of the injection light which can be represented by the injection ratio $R_{inj} = P_{inj}/P_{fr}$, which is ratio of the injection power to the output power of the free-running slave laser outside the laser cavity; another one is the detuning frequency Δf, which is the frequency difference between the CW master laser and the target mode of free running slave laser. First, the responses of the DLG-DBR laser with different detuning are investigated in Fig. 5 where the injection ratio R_{inj} is fixed to 0.13.

#256191 Received 21 Dec 2015; revised 2 Feb 2016; accepted 5 Feb 2016; published 16 Feb 2016

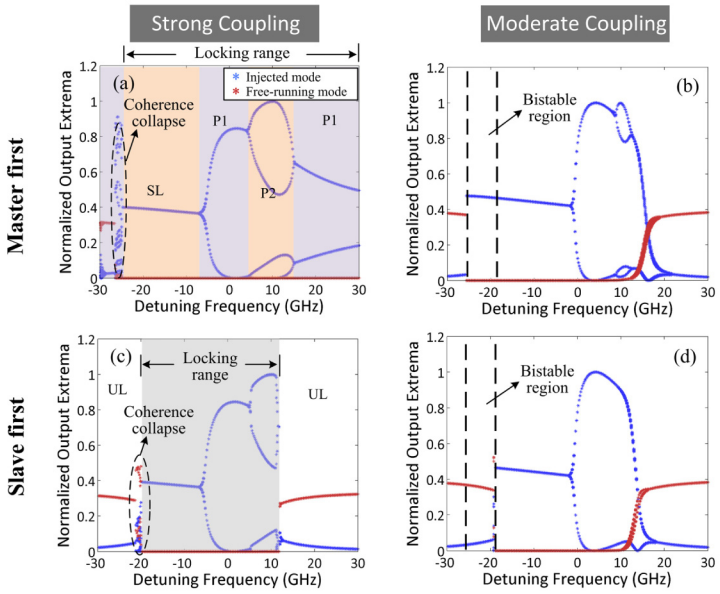

Fig. 5. Bifurcation diagram showing the equilibrium state extrema of the dimensionless field magnitude indicating the two lasing modes of the optically-injected DLG-DBR laser. For strong coupling case, $\varepsilon_{self} = 0.7 \times 10^{-23}$ m^3,$\varepsilon_{cross} = 1 \times 10^{-23}$ m^3; for moderate coupling case, $\varepsilon_{self} = \varepsilon_{cross} = 1 \times 10^{-23}$ m^3. The value of injection ratio $R_{inj} = 0.13$. The current of phase and grating section are biased at 6 mA and 10 mA respectively.

To investigate the behaviors of the OIL system under optical injection, the coupled differential Eqs. (1) and (2) are numerically solved using a fourth-order Runge-Kutta algorithm in time domain. The result of each simulation is characterized by the extrema observed on the temporal waveforms of all lasing modes [27] after long enough evolution time to ensure that the OIL system has converged to the stable solutions if they exist. The extrema found on the temporal waveforms versus the variations of detuning frequency are plotted in Fig. 5. The blue stars indicate the extrema found on the target mode of the injection and the red stars are found on the other mode of the dual-mode DLG-DBR laser. It is expected that bistability will be found in the optical injected DLG-DBR laser since such feature has been observed in many injection locking systems. To ensure that both of the bistable states can be successfully found in simulations, two different start-up sequences are used. In Figs. 5(a) and 5(b), the "master first" sequence is used where the light S_{inj} from the master laser is launched to the slave DLG-DBR laser first at $t = 0$, then after that the drive current I_a is injected to the active section of the slave DLG-DBR laser. With such start-up sequence, the slave laser will prefer to work at locked state in the bistable region. Otherwise, if I_a starts at $t = 0$ and S_{inj} starts when the slave has already been stable after the start-up relaxation oscillation, the slave laser will prefer to work at unlocked state as shown in Figs. 5(c) and 5(d) with "slave first" scheme. To investigate the impact of the mode coupling to the injection locking in the DLG-DBR laser, strong coupling scheme with $\varepsilon_{self} = 0.7 \times 10^{-23}$ m^3 and $\varepsilon_{cross} = 1 \times 10^{-23}$ m^3 is adopted in Figs. 5(a) and 5(c), and moderate coupling scheme with $\varepsilon_{self} = \varepsilon_{cross} = 1 \times 10^{-23}$ m^3 is adopted in Figs. 5(b) and 5(d). The currents of phase and grating sections are biased at 6 mA and 10 mA respectively in Fig. 5.

Figure 5(a) shows the multiple working regimes of the optical injected DLG-DBR laser with different detuning frequency at strong coupling and "master first" scheme. The slave laser works at free running state when $\Delta f < -25$ GHz. With the increasing of the detuning frequency, the laser passes through a narrow transition region with chaotic dynamics (coherence collapse) before entering the stable locking region. In the stable locking region,

#256191 Received 21 Dec 2015; revised 2 Feb 2016; accepted 5 Feb 2016; published 16 Feb 2016

the slave laser is locked to the injection signal to reach a steady state and thus a single extremum value is observed in the waveform of each mode. The stable locking region covers ~18 GHz and the extrema diagram of the locked mode bifurcates to two branches at $\Delta f = -7$ GHz. More than one extrema observed on a stable waveform means oscillations between the extrema. The two branches in the extrema diagram after the transition at $\Delta f = -7$ GHz correspond to the period-one (P1) oscillation state. The P1 oscillation will create a closed cycle in the phase diagram of (R_{inj}, Δf) plane [28]. With further increasing of the detuning frequency, the extrema diagram will bifurcate to four branches which correspond to the period-two (P2) oscillation state. The P2 oscillation state will come back to P1 state again when the detuning frequency is larger than 15 GHz. It should be emphasized that in the whole detuning region of -25 GHz $< \Delta f <$ 30 GHz, the laser mode without injection is fully suppressed. The working state transitions and the locking range are somewhat different in Fig. 5(c) when the "slave first" scheme is used. The first transition point from free running to stable locking is delayed to -20 GHz but the bifurcation point after the stable locking region is not changed. Instead of coming back to P1 state in "master first" scheme, the P2 oscillation state transits to the free running or unlocked (UL) state at $\Delta f = 11$ GHz with a fast growth of the mode without injection. When the moderate mode coupling scheme is used as shown in Figs. 5(b) and 5(d), there is a bistable locking region, similar with that with strong coupling shown in Figs. 5(a) and 5(c), but the transition processes are much cleaner without the chaotic dynamics. For stable locking region in Figs. 5(b) and 5(d), the right border is extended from -7 GHz to -2 GHz compared with strong coupling in Figs. 5(a) and 5(c), which benefits from the weaker mode coupling. The transition between the locked and free running states are easier in weak coupling scheme. In Fig. 5, we have shown the transitions between free running, stable locked, periodic oscillation and even chaotic states along the variation of tuning frequency. If we overlap the diagrams in Figs. 5(b) and 5(d), we can clearly observe the bistable region -25 GHz $< \Delta f < -20$ GHz which is between the different transition points in the two figures. Such bistable hysteresis curves have been used in many applications such as all optical signal processing [1]. Such hysteresis curves can be observed not only with the variations of detuning frequency, but also with the variations of the injection power or the injection ratio R_{inj}. The bifurcation dynamics versus the variations of injection ratio are shown in Fig. 6. We can clearly observe the bistable region ($9\% < R_{inj} < 21\%$) which is between the different transition points in the moderate coupling scheme as shown in Figs. 6(b) and (d). Similar bistable region also can be found in the strong coupling case but with a narrower region ($7\% < R_{inj} < 14\%$).

#256191 Received 21 Dec 2015; revised 2 Feb 2016; accepted 5 Feb 2016; published 16 Feb 2016

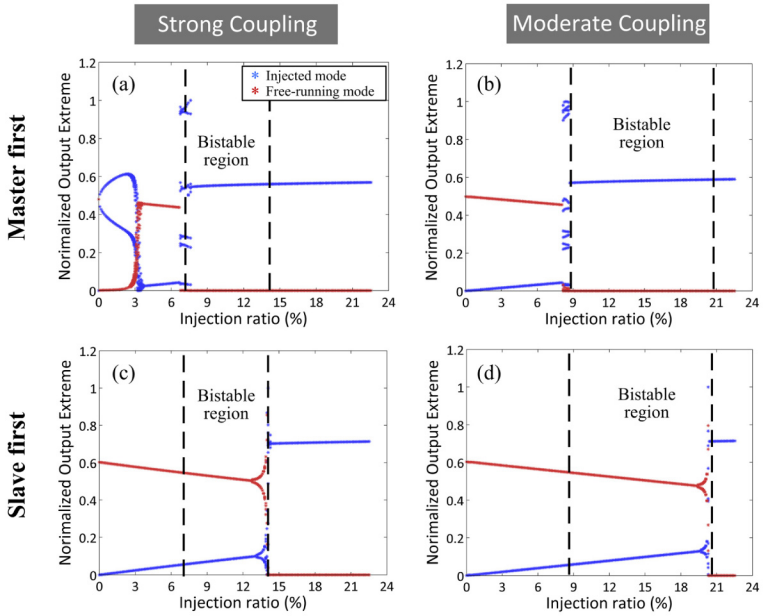

Fig. 6. Bifurcation diagram as a function of injection ratio indicating the two lasing modes of the optically-injected DLG-DBR laser. For strong coupling case, $\varepsilon_{self} = 0.7 \times 10^{-23}$ m^3,$\varepsilon_{cross} = 1 \times 10^{-23}$ m^3; for moderate coupling case, $\varepsilon_{self} = \varepsilon_{cross} = 1 \times 10^{-23}$ m^3. The value of detuning frequency $\Delta f = -20$GHz. The current of phase and grating section are biased at 6 mA and 10 mA respectively.

Obviously, the full map of the working states with variations of the detuning and injection ratio can be obtained by performing parameters sweeping and numerical simulations for each parameters combination. But such parameters sweeping is very time consuming and a much easier way is usually adopted if qualitative characterization of the system behavior is needed only. With the stationary form of Eqs. (2), (3) and (5) and neglecting the modes without injection, we can derive the steady solutions with respect to the photon density S_m, the phase ϕ_m and the carrier density N. The parameter ranges that steady state solutions exist will determine the locking range of the OIL system [20, 21]. Furthermore, the stability of such steady state solutions is characterized by linear stability analysis to determine the stable locking region. Finally, the injection locking map of the system is obtained as shown in Fig. 7. The results shown in Fig. 7 are not quantitatively accordant to those shown in Fig. 5 and Fig. 6 since we have neglected the modes without injection when we solve the steady state solutions where the system is equivalently mode decoupled with $\varepsilon_{cross} = 0$. The color bar indicates the normalized photon density S_m/S_{fr}. The photon density generally increases with the increasing of injection power and/or negative detuning. The impact of the detuning depends primarily on the nonzero α factor [29].

#256191 Received 21 Dec 2015; revised 2 Feb 2016; accepted 5 Feb 2016; published 16 Feb 2016

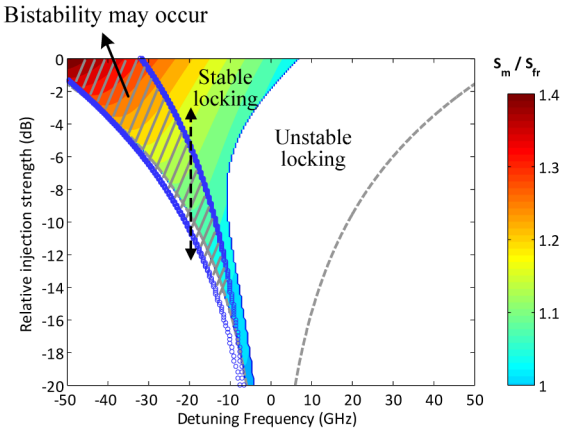

Fig. 7. Region of multiple stationary points on the injection-locking diagram

A region of the injection power and detuning frequency which providing the wavelength bistability of the dual mode device can also be found by the stationary analysis [25] as the shadow area shown in Fig. 7. From Fig. 7, the boundaries of the bistable region have defined the transition points between the free running, stable locking and the unstable locking states. For instance, as indicated by the vertical dashed line which crosses three working regions in the locking map, we can observe the hysteresis curves if the injection ration R_{inj} is tuned up and down along the arrow directions with fixed detuning frequency $\Delta f = -20$ GHz. The applications of such hysteresis curves will be discussed in the following section.

In this section, we have characterized the behaviors of the DLG-DBR laser with optical injection to one of the two lasing modes. The influences of the mode coupling, start-up sequences, frequency detuning, and injection ratio on the dynamics and bifurcations have been investigated. In fact, other parameters such as net mode gain, facet reflectivity and linewidth enhancement factor will also affect the injection locking dynamics of the dual mode laser but which are not the focuses of this paper.

4. High extinction ratio wavelength switching and optical memory

The results shown in Figs. 5, 6 and 7 have demonstrated the responses of the DLG-DBR laser to optical injection with different detuning frequencies and injection powers. Stable locking and bistability are both observed with either varying detuning frequency or injection ratio. Besides the on-off switching of the injected mode which can be found at the transition points in Fig. 5, another remarkable feature in Fig. 5 is the wavelength switching at the transition points. For the dual mode DLG-DBR laser, when the lower intensity mode of the free running two modes is chosen as the target mode, the mode switching at the transition point will greatly vary the mode suppression ratio $MSR = 10log(S_2/S_1)$. Such great changing of the MSR can provide a high extinction ratio wavelength switching which is desirable in optical communications and optical signal processing [1]. Moreover, the unique feature of the DLG-DBR laser is that the two wavelengths in switching can be widely tuned by controlling the drive currents of the grating and phase sections.

#256191 Received 21 Dec 2015; revised 2 Feb 2016; accepted 5 Feb 2016; published 16 Feb 2016

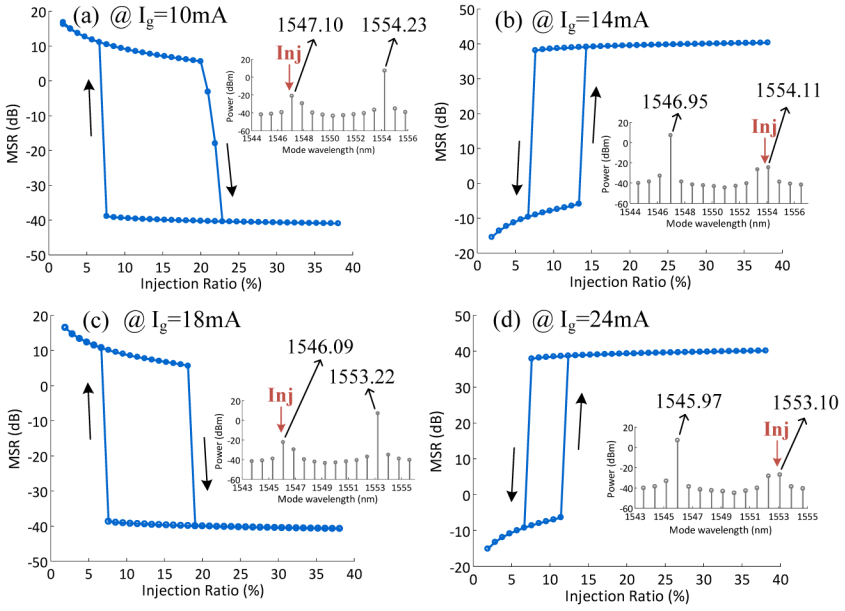

Fig. 8. The bistability characteristics of the injection locked double-layer grating DBR laser for the grating current I_g changes from 10 mA to 24 mA .The phase current is biased at 6 mA. The detuning frequency $\Delta f = -20$ GHz. The four insets indicate the spectrum of the modes in the laser which operates at unlocked state.

In Fig. 8, we show the hysteresis curves of the *MSR* versus injection ratio with the tuning of the grating currents of the DLG-DBR laser. The phase current is biased at 6 mA and the detuning frequency is fixed at −20 GHz in simulations. The transitions between the bistable states are indicated by arrows to differ the processes in the increasing and decreasing of the injection ratio. The four insets in the figure show the free running mode distribution and the selections of target mode. In Fig. 8(a) where I_g = 10 mA, the mode-1 oscillating at 1547.10 nm is the target mode and the mode-2 oscillating at 1554.23 nm is the free-running mode. By increasing and decreasing the injection ratio, wavelength switching with an MSR > 45 dB is achieved between the two bistable states. When I_g is increased from 10 mA to 14 mA, the target lower power mode at free running state switches from mode-1 to mode-2, which is accordant to the results shown in Fig. 3. Thus the two bistable states switch their positions with a slight wavelength blue-shift as shown in Fig. 8(b). In practice, such slight wavelength shift can further be compensated by adjusting the phase current. When I_g is increased to 18 mA, mode-1 becomes to the target mode again and mode hopping shifts the two modes by ~1 nm to 1546.09 nm and 1553.22 nm respectively. This bistable wavelength switching shown in Fig. 8(c) is similar to that in Fig. 8(a) with different working wavelengths. Such wavelength tuning can be repeated as shown in Fig. 8(d) and the more than 6 nm tuning range shown in Fig. 3 is fully available in the wavelength switching operations. As comparing with the wavelength bistability at three different wavelengths in an MG-Y laser reported in [30], the wavelength tuning ability of DLG-DBR laser for bistable wavelength switching is more flexible and powerful. Different operation wavelengths in the whole tuning window can be reached by changing the currents of grating and phase sections directly. The mode spacing between the two bistable states is determined by the two Bragg grating periods which can be adaptively designed in different applications.

The high extinction ratio wavelength switching shown in Fig. 8 can be used in many applications such as wavelength conversion in optical communications and all optical signal processing. One important application of the bistable wavelength switching is the optical memory. To demonstrate the dynamic switching process between the bistable states of the

#256191 Received 21 Dec 2015; revised 2 Feb 2016; accepted 5 Feb 2016; published 16 Feb 2016

DLG-DBR laser which is used as an optical memory element, we use the bistability characteristics in Fig. 8(a) as an example. Figure 9 shows the dynamic memory operations in which mode-1 and mode-2 act as the device output in response to the "set" and "reset" input signals. The optical injection signal is described by:

$$P_{inj}(t)=\begin{cases} P_{0/1}\pm\dfrac{1}{2}(P_1-P_0)\left\{1+\dfrac{t-\mu}{s}+\dfrac{1}{\pi}\sin\dfrac{t-\mu}{s}\pi\right\}, & \text{rising / failling edge} \\ P_{0/1}, & \text{pulse duration} \end{cases} \tag{6}$$

where P_0 and P_1 are powers at low and high levels of the optical injection signal, respectively. μ and s are the time parameters which define the rising and falling time. In our numerical modeling, the pulse duration is 3 ns and the rising and falling time are both 1 ns. Bright and dark pulses are used as the "set" and "reset" signals to control the laser with same bias power. The input signal will keep the bias power if no control signals are presented. From the right panel of Fig. 9, we can find that when a "set" pulse is injected at 10 ns, mode-1 switches from its original "OFF" state to "ON" state and maintains the "ON" state when the input signal drops back to the bias until the "reset" pulse appears at 18 ns. A 5 ns transition window for the "reset" pulse is required for the switching from "ON" state to "OFF" state of mode-1 which is limited by the growing speed of mode-2. Mode-1 will stay at "OFF" state after the "reset" signal until the next "set" pulse comes. At the same time, mode-2 shows opposite switching processes between "ON" and "OFF" states. The holding time of the memory is only dependent to the time intervals between "set" and "reset" pulses.

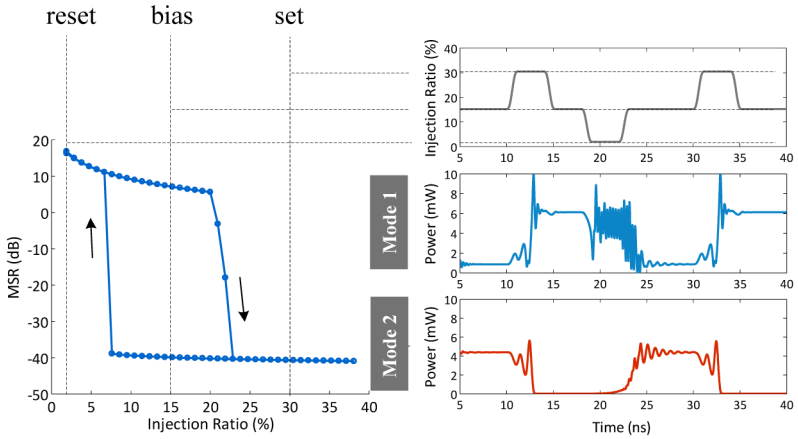

Fig. 9. Left panel: The bistability characteristics of the injection locked double-layer grating DBR laser, I_p = 6 mA, I_g = 10 mA. Right panels: Numerical intensity time traces of the injection ratio and of the two primary modes of the laser.

The memory operations can also be realized between any other groups of wavelengths due to the tuning characteristic of the DLG-DBR laser. This versatility in wavelength bistability is one of the most important advantages of the novel tunable dual mode laser comparing with other devices, and makes the DLG-DBR laser as a promising widely tunable optical logic device with great potential in all optical signal processing.

5. Conclusion

A novel tunable dual mode laser which employs a double-layer Bragg grating is proposed for the first time to our knowledge. The spacing of the two principle modes can be designed by controlling the double grating periods and more that 6 nm tuning range is demonstrated by changing the phase and grating currents. The responses of the DLG-DBR laser to different

#256191 Received 21 Dec 2015; revised 2 Feb 2016; accepted 5 Feb 2016; published 16 Feb 2016

optical injections and corresponding bifurcation characteristics of the laser are investigated. The influences of mode coupling strength, start-up sequences, injection ratio, and the detuning frequency are all characterized. The mode switching in the transitions shows a possible way to realize high extinction ratio bistable wavelength switching. Hysteresis loops with $MSR > 45$ dB are obtained by control the injection ratio to the DLG-DBR laser. Such hysteresis loops for bistable wavelength switching can be obtained in a 10 nm tuning window by controlling the driving currents. Furthermore, optical memory operations based on the injection bistability of the DLG-DBR laser are demonstrated numerically. In principle, such memory operations can be realized freely in the 10 nm tuning range. Thus the DLG-DBR laser can be used as a novel optical logic gate device for in-plane all-optical signal processing. Such simple and cost-effective tunable dual mode lasers will also find many potential applications in optical communications, all-optical signal processing such as optical memory, flip-flop operations and self-routing networks.

Acknowledgments

This work was supported in part by the National High Technology Developing Program of China under Grant No. 2013AA014503, the National Natural Science Foundation of China (NSFC) under Grants 11174097 and 61475131, the International S&T Cooperation Program of China under Grant 1016, and the Hong Kong Research Grants Council under Grant PolyU5263/13E.

#256191 Received 21 Dec 2015; revised 2 Feb 2016; accepted 5 Feb 2016; published 16 Feb 2016